Green Chemistry

ROYAL SOCIETY OF CHEMISTRY

PAPER

View Article Online
View Journal | View Issue

Cite this: *Green Chem.*, 2023, **25**, 7166

Efficient algal lipid extraction *via* a green bio-electro-Fenton process and its conversion into biofuel and bioelectricity with concurrent wastewater treatment in a photosynthetic microbial fuel cell†

Swati Das,[a] Rishabh Raj [b] and Makarand M. Ghangrekar *[a,b,c]

Third-generation biodiesel produced using carbon-neutral algal feedstock is a promising alternative to meet global energy demands. However, the economic viability of algae-derived biodiesel is severely impacted by poor lipid recovery and taxing downstream processes. In this regard, green Fenton chemistry was employed to disrupt algal cells in a bio-electro-Fenton-assisted photosynthetic microbial fuel cell (BEF-PMFC) by employing different Fenton catalysts for higher lipid recovery. The maximum lipid yield of 39.2% with 98% chlorophyll removal was achieved by homogeneous Fenton oxidation in a Ni–Pd/C catalysed BEF-PMFC after 6 h of reaction at a pH of 3.0, whereas a comparable lipid yield (37.5%) and chlorophyll removal (95%) were attained by a CoFe-AC-driven heterogeneous Fenton oxidation process. Experiments exhibited a maximum of 90% lipid extraction efficiency, which was 1.5-fold higher than that without cell-disruptive wet biomass. Finally, biodiesel synthesised from lipids obtained *via* BEF conformed to the ASTM D6751-12 standard. The PMFC equipped with the Ni–Pd/C coated cathode generated a maximum power density of 74.5 mW m^{-2} and a chemical oxygen demand removal efficiency of 89.2%, which were *ca.* 2.8 times and 1.2 times higher compared to the control PMFC operated without any catalyst on the cathode. Thus, this investigation paves the way for using a green chemistry-based strategy to assist PMFCs in achieving higher recovery of bioelectricity and lipid recovery with minimal reliance on chemicals.

Received 10th May 2023,
Accepted 3rd August 2023

DOI: 10.1039/d3gc01548c

rsc.li/greenchem

1. Introduction

The exploration of sustainable alternatives to fossil fuels to meet surging energy demands seeks to satisfy an apparent research gap.[1] Therefore, researchers are hunting for alternative renewable biofuels due to the impending depletion of fossil fuels and the ensuing environmental repercussions.[2,3] In this regard, oleaginous microalgal biomass is considered a potential feedstock for generating third-generation carbon-neutral biofuels and other valuables that cater to the energy demand as well as address ecological concerns.[4] Generally, the microalgal lipid content is 20–50% of their total dry weight, which can be converted to biodiesel after transesterification. Cultivation, harvesting, and lipid extraction of algal feedstock make up to 90% of the total biofuel production cost, of which 30 to 40% is contributed by the lipid extraction process alone.[5,6] Moreover, different physicochemical drying processes are generally employed to recover lipids from microalgae; unfortunately, biomass drying damages saturated fatty acids, producing lower grade biodiesel. Additionally, enormous energy consumption during drying makes this process economically infeasible.[7] Hence, lipid extraction from wet biomass, which by-passes the drying step, has drawn plenty of interest among aspiring researchers for the successful commercialisation of algal biodiesel production.[6,8] However, damp lipid extraction often requires additional pre-treatment that aims to disrupt rigid cell walls to obtain high-quality lipid yields. Furthermore, when the chemical solvent is applied, wet microalgal cells tend to endure in the water phase as their surface charges prevent contact with the organic solvent phase. Due to

[a]*PK Sinha Centre for Bioenergy & Renewables, Indian Institute of Technology Kharagpur, Kharagpur, 721302 West Bengal, India.*
E-mail: ghangrekar@civil.iitkgp.ac.in
[b]*School of Environmental Science and Engineering, Indian Institute of Technology Kharagpur, Kharagpur, 721302 West Bengal, India*
[c]*Department of Civil Engineering, Indian Institute of Technology Kharagpur, Kharagpur, 721302 West Bengal, India. Tel: +91 3222 283440*
† Electronic supplementary information (ESI) available. See DOI: https://doi.org/10.1039/d3gc01548c

the immiscibility of water with organic solvents, direct lipid recovery from untreated wet algae provides lower yield and poor quality of lipids. Apparently, this phenomenon can be alleviated by disrupting the algal cell wall to readily release the internal lipids, thus facilitating the accessibility of lipids after evaporation of the solvent. Nonetheless, the majority of the physical disruption techniques rely on high energy consumption due to a continuous supply of thermal, electrical, or mechanical energy inputs until the cell wall is shattered, rendering it impracticable for scaling up. Hence, emphasis has been given on the invention of an advanced cell lysis strategy that possesses desired characteristics, including higher lipid extraction efficiency, minimal lipid oxidation and destruction, and modest energy intensity with highly qualitative biodiesel properties.[9]

In this regard, the electro-Fenton reagent, which comprises a mixture of electrogenerated *in situ* H_2O_2 and Fe^{2+} with the utilisation of an external potential, has been employed for algal cell disruption due to its economical operation and non-toxic properties. Additionally, hydroxyl free radicals ($^{\bullet}OH$), the incredibly reactive oxygen species (ROS) generated in the electro-Fenton reaction, disrupt algal cell walls by targeting organic components such as glycoproteins, polysaccharides, cellulose, and phospholipids (eqn (1)).

$$Fe^{2+} + H_2O_2 \rightarrow Fe^{3+} + OH^- + {}^{\bullet}OH \quad (1)$$

Unlike the traditional Fenton process, H_2O_2 is electrosynthesised in the electro-Fenton process by using carbon electrodes that inherently favours the $2e^-$ oxygen reduction reaction (ORR) due to weak oxygen binding energy as presented in eqn (2). Such materials have more affinity towards *OOH rather than *O (eqn (3)), which is pivotal in manoeuvring the ORR for H_2O_2 generation.[10] Using carbon nanomaterials with a high specific surface area (more ORR active sites) like activated carbon (AC), carbon nanotubes, and graphene can boost the H_2O_2 yield.[11,12] Alternatively, metals which feature similar properties such as Ni and Pd have been employed for H_2O_2 electrosynthesis.[13]

$$\begin{aligned} &O_2 + 4H^+ + 4e^- \rightarrow {}^{*}OOH + 3H^+ + 3e^- \rightarrow \\ &{}^{*}O + 2H^+ + 2e^- + H_2O \rightarrow \\ &{}^{*}OH + H^+ + e^- + H_2O \rightarrow 2H_2O \end{aligned} \quad (2)$$

$$O_2 + 2H^+ + 2e^- \rightarrow *OOH + H^+ + e^- \rightarrow H_2O_2 \quad (3)$$

Carbon catalysts when coupled with Fe or its composites with other transition metals like Ni, Co, and Mn can perform the dual role of H_2O_2 production and its simultaneous decomposition to $^{\bullet}OH$ *via* the famous Fenton reaction (eqn (1)). This ensures perennial production of transient $^{\bullet}OH$ in the cathodic chamber of a bio-electro-Fenton (BEF) system leading to the oxidation of target compounds.

Sandani *et al.* (2022) demonstrated that the electro-Fenton reaction is highly effective in enhancing the lipid yield (highest 19.99 ± 1.33% w/w) from wet microalgal biomass in comparison to other conventional methods.[14] Moreover, the comprehensive reduction of major biodiesel impurities such as chlorophylls through the reaction with ROS is an additional advantage of electro-Fenton reaction-based cell lysis. Additionally, implementation of the electro-Fenton treatment has been proven to have positive effects on the lipid profile for the production of high-quality biodiesel, including a reduction in polyunsaturated fatty acids (PUFA) and an increase in saturated fatty acids (SFA) and monounsaturated fatty acids (MUFA).[15] Daghrir *et al.* (2014) reported a yield of 55.3% lipid per g of dry biomass of *Chlorella vulgaris via* electrochemical oxidation at an applied current intensity of 0.6 A in just 60 min of operation using a Ti/IrO_2 anode and stainless-steel cathode.[16] However, the electricity input for the electro-Fenton system makes this technology energy intensive and uneconomical, compromising with its scalability.

To alleviate this major drawback, an innovative bio-electrochemical reactor has been developed in which oxygen reacts with two electrons, produced by microorganisms in the anodic chamber, to form H_2O_2 and induce a BEF reaction together with Fe^{2+} present in the cathodic chamber. Besides, the BEF reaction eliminates storage and transportation limitations associated with the traditional Fenton method for H_2O_2 and avoids the generation of vast quantities of Fe sludge by consistently regenerating Fe^{2+} at the cathode by reducing Fe^{3+}.[17] Furthermore, a prolonged reaction time with highly active ROS results in lipid degradation (Fig. S1†), thereby necessitating a gentle cell disruption mechanism that inhibits further lipid dilapidation without affecting its fuel properties.

In this context, the present investigation aims to demonstrate lipid extraction from wet algal biomass utilising green Fenton oxidation in a BEF-assisted photosynthetic microbial fuel cell (BEF-PMFC). Simultaneously, employing nickel–palladium on carbon (Ni–Pd/C), cobalt–iron with activated charcoal (CoFe-AC), and activated charcoal-Fe_2O_3 (AC-Fe) as cathode catalysts in the BEF-PMFC boosted bioelectricity generation and wastewater treatment, thus manifesting the dual advantages of these nanocomposites. To the best of our knowledge, the current exploration is the first on a BEF-mediated cell disruption process for copious lipid recovery from wet algal biomass. Furthermore, the direct lipid extraction from wet biomass of algae eliminates the biomass harvesting process, making this procedure more affordable than conventional physicochemical methods. In addition, the comparative efficacy of heterogeneous and homogeneous BEF catalysts for accelerated ROS production for algal cell lysis in a wide pH range has not been investigated to date. Furthermore, to ensure the quality of the produced biodiesel, bio-oil recovered from the BEF-PMFC was analysed and compared with the standard data of ASTM D6751-12 and EN 14214:2012. Evidently, BEF-PMFC is a self-driven, low-carbon footprint, and scalable technique that can be adopted for the mass production of algal biodiesel in the future. Hence, the concept of concurrent recovery of biodiesel and bioelectricity along with wastewater treatment facilitated through a single system of a BEF-PMFC is commercially lucrative and can be a plausible renewable alternative approach for depleting fossil fuel resources (Fig. 1).

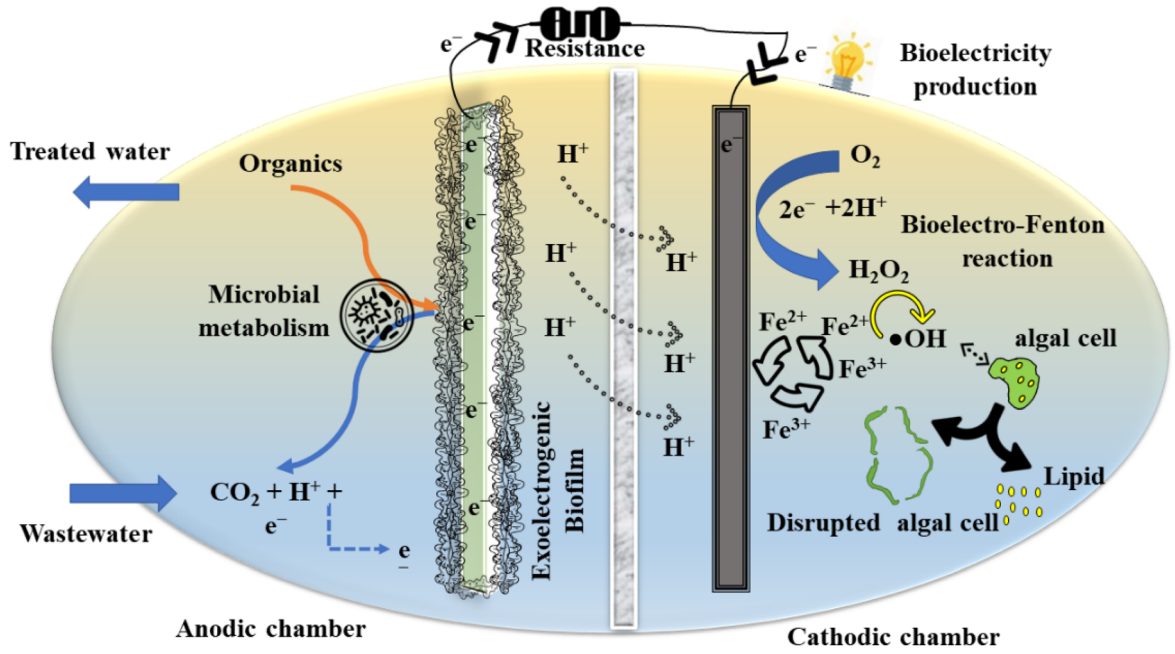

Fig. 1 Schematic diagram of a bio-electro-Fenton-assisted photosynthetic microbial fuel cell.

2. Materials and methods

2.1 Fabrication of double chamber BEF-PMFCs

Three double chamber PMFCs were fabricated, having anodic and cathodic chambers separated by a proton exchange membrane (PEM) (Nafion 117 (DuPont, USA)) (Fig. S2†). Each PMFC, fabricated using an acrylic sheet, consisted of two distinct chambers with a working volume of 90 mL each making the total volume of each setup to 180 mL. Both the anode and cathode of the BEF-PMFCs were made up of carbon felt (projected surface area of 4 cm × 4 cm each) and were connected with an external resistance of 100 Ω using stainless steel wire. The produced electrons and protons from the anodic chamber of PMFCs were transferred to the cathodic chamber through an external circuit and PEM, respectively. The three PMFC cathodes were coated with Ni–Pd/C, CoFe-AC, and AC-Fe catalysts separately and termed BEF-PMFC-T1, BEF-PMFC-T2, and BEF-PMFC-T3, respectively (Table S1†). Accordingly, the bare carbon felt without having any cathode catalyst coating was also operated as the control PMFC-C to facilitate performance comparison with the other three PMFCs.

The mixed anaerobic consortium collected from the septic tank (located in the residential area of IIT Kharagpur) was utilised as an inoculum of electricigens after heat pre-treatment to overcome the methanogenesis. However, the mixed algal consortium was cultured in the cathodic chamber of all the PMFCs. Sucrose-based synthetic wastewater with a chemical oxygen demand (COD) of 3 g L^{-1} was utilised as the anolyte for all PMFCs. The retention time of synthetic wastewater in the anodic chamber of the setup was three days, and both the initial and final COD of the anolyte were measured after each feed cycle.[18]

2.2 Cultivation of algae in the cathodic chamber of PMFCs

The mixed consortium of freshwater microalgae was collected from the algal raceway pond located at the IIT Kharagpur campus. The collected algal consortium was allowed to develop for a period of 5 days with periodic addition of BG-11 medium.[18] The optical density of the algal culture at 682 nm (OD_{682}) was measured daily using a spectrophotometer (PG Instruments, China). The mixotrophic algal cultivation in the cathodic chamber of PMFCs was inoculated with 0.5 g L^{-1} of mixed algal biomass at 30 ± 5 °C. The algal culture was grown in the cathodic chamber of PMFCs under cool white fluorescent light with a light intensity of 7000 lux for 18 : 6 h of light: dark photoperiod, supplemented with ambient air (@1 L min^{-1}) by employing an aquarium pump (SOBO Aquarium air pump, China). Algal biomass was determined using dry cell weight, and the overall biomass productivity (g L^{-1} day^{-1}) was estimated from the variation in the biomass concentration (g L^{-1}) as described in our previous investigation.[18]

2.3 Synthesis of Fenton catalysts for algal cell disruption

The AC-Fe composite was prepared by blending Fe_2O_3 nanopowder with powder-activated charcoal (AC) in a ratio of 60 : 40 (by wt). The AC is a well-known catalyst used for the electrogeneration of H_2O_2, while Fe_2O_3 catalyses the *in situ* produced H_2O_2 into $^{\bullet}OH$, the chief oxidant in the Fenton oxidation-based process. Similarly, the Ni–Pd catalyst was selected due to its high selectivity for H_2O_2 generation. It was prepared by mixing Ni nanoparticles with Pd/C (10% by wt) in a weight ratio of 50 : 50. Also, 10 mg L^{-1} of Fe^{2+} was added to the catholyte in the form of $Fe_2SO_4{\cdot}7H_2O$ to catalyse the production of $^{\bullet}OH$ homogeneously.

Fe and Co were selected to yield higher $^{\bullet}OH$ by the dual action of Co that can produce and activate H_2O_2 simultaneously.[19,20] The Fe–Co composite catalyst was synthesised *via* a controlled co-precipitation method. One gram of Fe–Co catalyst (2 : 1 by wt) was prepared by taking stoichiometric amounts of $CoCl_2{\cdot}6H_2O$ and $FeCl_3{\cdot}6H_2O$ salts and dissolving them in 100 mL of distilled water separately. Furthermore, the Fe and Co solution was transferred to a 500 mL beaker and sonicated for 30 min. The pH of the mixture solution was then increased to 11.0 by dropwise addition of 1 M NaOH solution. The colour of the Fe–Co solution turned dark as the pH increased, and the reaction was allowed to continue for 2 h at 80 °C under constant stirring. Sufficient time was provided for the solids to settle, which were magnetically collected after discarding the supernatant. The precipitate was washed several times with deionised water and ethanol until the pH of the supernatant became close to neutral. The washed solids were dried overnight in a hot air oven at 80 °C. Ultimately, the dried particles were calcined at 400 °C for 2 h in a muffle furnace resulting in the formation of $CoFe_2O_4$ particles. $CoFe_2O_4$ was further blended with AC in a 60 : 40 ratio by weight to boost *in situ* H_2O_2 electro-generation, curtailing accelerated $^{\bullet}OH$ formation.

2.4 Preparation of catalyst-modified cathodes

All the cathodes used in the BEF-PMFCs were fabricated using carbon felt as the base material, pre-treated using 1 M HCl solution, followed by vigorous cleaning with deionised water and acetone. Prior to use, pre-treated felts were dried in a hot air oven at 100 °C. The catalyst amount was calculated by fixing a loading of 2 mg cm^{-2} of the cathode surface area, whereas Nafion binder loading was 6.67 μL mg^{-1} of catalyst, and the quantity of these materials was estimated accordingly. For each catalyst, an ink-based solution was prepared by adding the catalyst, binder, and acetone in the requisite proportion and mixed in an ultrasonic bath with a rating of 120 kHz for 2 h. The homogeneous ink-based solution was painted over the cathode surface uniformly and then dried at 80 °C for 12 h before installing the coated cathodes in the PMFC reactor.

2.5 Characterisation of different catalysts used for cell disruption

The shape, size, and arrangement distribution of all three Fenton catalysts were analysed by field emission scanning electron microscopy (FESEM).[21] Also, energy-dispersive X-ray (EDX) (ZEISS EVO 60, Carl ZEISS SMT, Germany) spectrum analysis was performed to confirm the presence of elements and atomic proportions in the Fenton catalyst using an EDX spectrometer. Moreover, the crystalline structure and diffraction patterns of Ni–Pd/C, CoAC-Fe, and AC-Fe were analysed using an X-ray diffractometer (D8 Focus Bruker, Karlruhe, Germany) under the scanning range in the 2θ region from 20° to 80°. Furthermore, Fourier transform infrared (FTIR) spectroscopy (Thermo Fisher Scientific, NICOLET 6700, USA) was performed to identify the active functional group and bands present in these three Fenton catalysts.

2.6 Optimisation of catalyst-based algal cell disruption and lipid recovery in the BEF-PMFCs

Microalgae cultivated in the cathodic chamber of the PMFCs were initially harvested by centrifugation to estimate the weight of concentrated wet biomass after the culture reached the stationary growth phase. After that, homogeneous Ni–Pd/C and heterogeneous CoAC-Fe and AC-Fe were coated on the cathode of the respective PMFCs to initiate the BEF reaction for algal cell disruption. Different relevant parameters, such as retention time (0–24 h) and pH (3.0–9.0), were optimised to estimate higher cell disruption and lipid recovery. Consequently, the concentration of produced H_2O_2 in the catholyte was also quantified using the colorimetric method suggested by Graf and Penniston *et al.* (1980).[22] After the optimised duration, the catholyte containing suspended algal lipid was separated by the Soxhlet extraction process (*n*-hexane : disrupted biomass; 1 : 1).

2.7 Characterisation of the *in situ* generated H_2O_2 and $^{\bullet}OH$

The quenching test was performed using methylene blue (MB) to confirm the presence of $^{\bullet}OH$ in the BEF system. The residual concentration of MB was measured by recording the absorbance at λ_{max} = 650 nm using a UV-visible spectrophotometer and the production of $^{\bullet}OH$ was further confirmed by performing pulsed electron paramagnetic resonance (EPR) spectroscopy (Bruker, ELEXSYS 580, USA).

2.8 Extraction and estimation of chlorophyll content

To estimate chlorophyll, 2 mL of algal biomass was centrifuged at 8000 (14 160*g*) rpm for 10 min. After discarding the supernatant of the culture, the pellet portion was mixed with 2 mL of methanol, sonicated for 30 s, and again centrifuged at 8000 (14 160*g*) rpm for 5 min. After that, total chlorophyll concentration containing chlorophyll-a and chlorophyll-b was checked using a spectrophotometer (PG Instruments, China) at 665.2 and 652.0 nm, respectively, and total chlorophyll concentration was estimated using eqn (4).

$$\mathrm{Ch} - (a+b) = 22.12A_{652.0} + 2.71A_{665.2}\ \mu\mathrm{g\ ml^{-1}} \quad (4)$$

where Ch − (a + b) denotes total chlorophyll content, and $A_{652.0}$ and $A_{665.2}$ are the absorbances at 652.0 nm and 665.2 nm, respectively. Moreover, the percentage removal of chlorophyll was estimated based on the concentration obtained after the periodic time of the BEF reaction.

2.9 Algal cell disruption quantification *via* hemocytometry

Hemocytometry was carried out to count the total viable algal cells with the assistance of an optical microscope under a magnification of 100× objective resolution (Olympus Optical, Tokyo, Japan). Also, Trypan blue dye was utilised to determine the number of living algal cells after BEF-assisted cell disruption as reported in Prajapati *et al.* (2015).[23] The algal cell death

(%) was estimated from eqn (5). The microscopic images of the intact algal cells and after cell disruption by employing the three Fenton catalysts are shown in Fig. S3.†

$$\text{Algal cell death}\,(\%) = \frac{(X_0 - X_t)}{X_t} \times 100 \quad (5)$$

where X_0 and X_t are the viable algal cell biomass (cells per mL) at times 0 and t during the BEF reaction.

2.10 Estimation of total lipid content and lipid recovery efficiency

The algal lipid components, along with the disrupted cell were recovered from the cathodic chamber of all BEF-PMFCs adopting an optimised cell hydrolysis time. Thereafter, the crude lipid yield (mg g^{-1} of biomass) was separated from lysed biomass using the Soxhlet method.[18] The lipid yield after cell disruption was determined by quantifying lipids from eqn (6).

$$\text{Lipid yield}\,(\%) = \frac{\text{Extracted lipid after BEF reaction (mg)}}{\text{Total lipid content present in microalgae (mg)}} \times 100 \quad (6)$$

The efficiency of lipid extraction was also estimated as per the method described by Park *et al.* (2014).[24] In a nutshell, *n*-hexene was mixed with the suspension of lysed cells (1 : 1), and the mixture was agitated for 60 min at 120 rpm. Afterwards, the solvent containing the lipid layer was separated by centrifugation at a speed of 1500 rpm for 10 min, followed by evaporation to collect algal lipids (EZ2 plus, Geneva, UK). The lipid-rich solution was recovered followed by the additional treatment of remaining solid particles with ethanol for 30 min under stirring to extract leftover lipids in the solid phase. After that, most of the impurities, including extra reactants and proteins, remained in the aqueous phase while the refined lipids were stored in the hexane phase. Finally, the lipids were obtained from the hexane phase through evaporation using a rotary evaporator.[25] The percentage weight of lipids extracted from the wet biomass was obtained as per eqn (7).

$$\text{Lipid extraction efficiency}\,\% = \frac{\text{Weighed lipid after evaporation}}{\text{total lipid content after harvested biomass}} \quad (7)$$

2.11 Characterisation of algal lipid and leftover biomass through GC-MS and FTIR

After an optimised duration of the Fenton reaction, the algal lipid components collected from the cathodic chamber of the PMFCs were subjected to the transesterification process.[26] Afterwards, the fatty acid methyl ester (FAME) components were separated from the lysed algal cell biomass and were subsequently identified using a gas chromatograph (GC) (Thermo Fisher Scientific, USA) coupled with a mass spectrometer (MS) (Agilent Technologies MS-5977B, Penang, Malaysia). Full-scan analysis was performed in the mass range of 30 to 400 m/z as described by Das *et al.*[26] The crude algal lipid after transesterification and lipid extracted residual biomass were subjected to characterisation through FTIR to identify different functional groups present in both the samples. Full scan analysis was performed in the wavelength ranging from 500 cm^{-1} to 3000 cm^{-1}, as described by Das *et al.*[26]

2.12 Estimation of biodiesel quality parameters

The FAME profiles of algal lipids recovered *via* BEF-assisted cell disruption methods were used to assess biodiesel quality parameters. Following equations (eqn (8)–(14)) were used to determine iodine value (IV), saponification value (SV), gross calorific value (GCV), cetane number (CN), kinematic viscosity (ν), oxidative stability (OS) and degree of unsaturation (DU).[27]

$$\text{Iodine value (IV)}\,(\text{mg } I_2/1\text{ g lipid}) = \sum \frac{254 \times D \times A}{\text{MW}} \quad (8)$$

$$\text{Saponification value (SV)}\,(\text{KOH mg}/1\text{ g of lipid}) = \sum \frac{560 \times A}{\text{MW}} \quad (9)$$

$$\text{Cetane number (CN)} = 46.3 + \left(\frac{5458}{\text{SV}}\right) - 0.225 \times \text{IV} \quad (10)$$

$$\text{Calorific value (CV)} = 49.43 - 0.041 \times \text{SV} - 0.015 \times \text{IV} \quad (11)$$

$$\text{Kinematic viscosity}\,(\text{mm}^2\,\text{s}^{-1}) = \exp \sum w(-12.503 + 2.496 \ln(\text{MW}) - 0.17D) \quad (12)$$

$$\text{Oxidative stability (OS) (h)} = (117.92/X) + 2.5905 \quad (13)$$

$$\text{Degree of unsaturation}\,(\%\text{ w}) = \sum (\text{MUFA} + 2 \times \text{PUFA}) \quad (14)$$

where w, D, A, and MW represent the weight fraction, number of double bonds, % composition, and the molecular mass of the ith FAME present in algal cells, respectively, whereas X, MUFA, and PUFA are total weight % of linoleic and linolenic acid, monounsaturated and polyunsaturated fatty acid.

2.13 Bioenergy recovery and wastewater treatment

The influent and effluent collected from the anolyte of all PMFCs were examined to assess the organic matter removal efficiency from the perspective of COD reduction using the closed reflux colorimetric method.[28] Moreover, the quantity of chemical energy that was converted into electrical energy through the PMFCs from the theoretical maximum electrical energy was estimated *via* coulombic efficiency (CE).[29] The operating voltage (OV) across 100 Ω of external resistance and open circuit voltage (OCV) under no current flowing conditions for the four PMFCs were periodically recorded using a data acquisition/switch unit (Agilent Technologies, Penang, Malaysia) coupled with a computer system. The data for polarisation graphs were generated by varying the external resistance from 50 kΩ to 10 Ω using a resistance box (GEC05R Decade Resistance Box, Bengaluru, India). The power density was expressed as power produced per m^2 area of the cathode

in mW m^{-2}. The maximum power density and internal resistance of the PMFCs were evaluated using polarisation after the PMFCs attained stable electrical performance and COD removal efficiency. The internal resistance of all PMFCs was calculated from the slope of the voltage *vs.* current plot obtained during polarisation.

3. Results and discussion

3.1 Biomass growth and macromolecular composition of algae

The wet weight of green algal biomass was estimated through a calibration plot between weight of wet biomass (W_{wt}) and optical density ($OD_{682\ nm}$) as elucidated by eqn (15). A decent linear relationship was observed between W_{wt} and optical density of mixed algal consortium with a significant coefficient (R^2) value of 0.998 by dosing the initial biomass concentration at 0.6 g L^{-1} in BG11 medium. Also, a correlation between W_{wt} subjected to disruption and the corresponding dry weight content (D_{wt}) was evaluated using eqn (16).

$$D_{wt}\ (g\ L^{-1}) = 0.362 \times OD_{682\ nm} + 0.002 \quad (15)$$

$$D_{wt}\ (g\ L^{-1}) = 0.15 \times W_{wt} \quad (16)$$

In this investigation, the lag phase was noticed in the first two days due to the acclimatisation of algae in the cathodic chamber of all PMFCs. After 24 h of cultivation, the exponential growth phase was observed, and the maximum W_{wt} of 2.8 g L^{-1} was achieved after 5 days of cultivation with BG 11 medium at 7000 lux of light intensity sparged with atmospheric air (@1 L min^{-1}). Moreover, the specific growth rate of 0.3 per day with the total biomass productivity of 0.4 g L^{-1} day was achieved in the PMFCs. Furthermore, mixed algal consortium cultivated in the cathodic chamber of the PMFCs had 55.3 μg mL^{-1} chlorophyll yield and a maximum of 41.3% w/w lipid content, which was corroborated with the finding of Gerbens-Leenes *et al.* (2013).[30]

3.2 Characterisation of BEF catalysts using XRD, FTIR and SEM

The XRD analysis of the Fe nano-powder and AC composite showed a series of diffraction peaks pertaining to Fe in addition to a broad peak anchored at 26.03°, which could be indexed to the amorphous carbon of AC (Fig. 2). The distinct and sharp peaks attributed to the (220), (311), (400), (422), (511) and (440) lattice structures of maghemite (γ-Fe_2O_3) correspond to the peak positions at 30.1, 35.6, 43.2, 53.8, 57.2 and 62.8°, respectively. These values coincide with the standard crystal data for γ-Fe_2O_3 (JCPDS No. 39-1346) and confirm even blending of Fe nano-powder and AC.[31] Moreover, the absence of any unwanted peaks attests to the purity of the AC-Fe mixture. A similar XRD spectrum of maghemite blended with carbon was reported in a past investigation by Lu *et al.* (2019).[32]

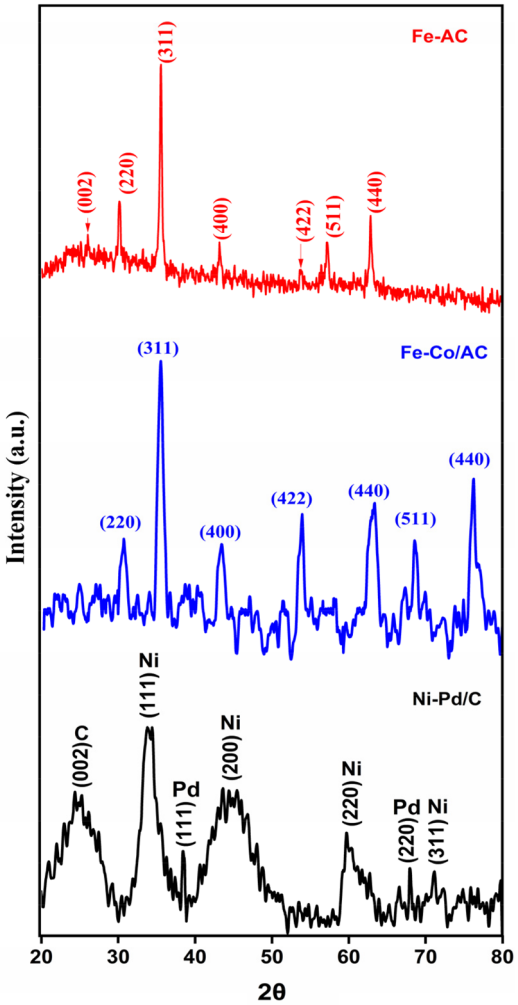

Fig. 2 The XRD spectrum of AC-Fe (red); CoFe-AC (blue); and Ni–Pd/C (black) catalysts with the respective planes.

The XRD spectrum of the synthesised Co–Fe composite confirms the formation of the spinel lattice structure of $CoFe_2O_4$ matching the standard data (JCPDS. No 22-1086).[33] Specifically, the Bragg peaks resemble the cubic spinel crystal phase corresponding to lattice planes of (220), (311), (400), (422), and (511) at 2θ values of 29.9°, 35.5°, 43.4°, 53.9°, and 62.8°, respectively (Fig. 2). Furthermore, the high synthesis temperature results in the formation of nano-sized crystals of $CoFe_2O_4$, which is also evident from the sharpness of the diffraction peaks.[34] The spectra did not contain any unwarranted peaks, which indicates that the as-synthesised catalyst was not adulterated. These observations are in corroboration with the previously reported findings of spinel cobalt ferrite composites.[35]

The Ni–Pd/C composite revealed a distinct peak of each element in the XRD spectra. A broad diffraction peak centred at 24.3° represents the typical reflection of the (002) plane of the amorphous carbon.[36] The lattice planes of (111), (200), (220), and (311) at 2θ values of 33.8°, 43.6°, 59.8°, and 71.1°, respectively, are the characteristic peaks of metallic Ni par-

ticles (Fig. 2). However, these peaks were significantly broader, which may be because of blending with Pd/C. Similar broadened peaks of Ni were observed when activated carbon was used as the support.[37] In addition, the presence of Pd in the composite was indicated by diffraction peaks at 38.4 and 68.0° corresponding to the (111) and (220) lattice planes of the Pd nanoparticles.[38] Notably, Pd also produces a prominent peak around the 2 θ value of 45° depicting the lattice plane of (200), although it cannot be observed in the FTIR spectra, which probably may be due to the overlapping peak of Ni. Nonetheless, these findings indicate that the Pd/C crystal has a face-centered cubical structure.[39]

The FTIR spectra were used to identify the functional group present on the surface of the composite catalysts (Fig. 3). A broad peak around the wavenumber 3300 to 3600 cm^{-1} represents the typical OH group adsorbed on the carbonaceous materials while peaks appearing around 1550 cm^{-1} and 1020 cm^{-1} could be due to the stretching vibration of C=C or C–O bonds, respectively.[40] Furthermore, Fe–O–Fe vibrations resulted in a peak at 800 cm^{-1}, whereas the peak at 692 cm^{-1} and 549 cm^{-1} can be ascribed to the stretching and bending vibration of Fe–O of γ-Fe_2O_3.[41,42] Similarly, overlapping bands at the wavenumber of 562 cm^{-1} and 538 cm^{-1} appear due to the vibration of the tetrahedral site of the $CoFe_2O_3$.[43] The bands due to the octahedral site vibration of the spinel ferrites usually emerge in the range of 500–400 cm^{-1}, although it is not visible in the FTIR spectra due to the limitation of the instrument (Fig. 3A). The peaks at wavenumbers 1338 cm^{-1} and 1644 cm^{-1} can be attributed to the bending vibration of C–O and C–H bonds, respectively.[44] A blunt peak of adsorbed O–H centred around the wavenumber 3350 cm^{-1} was also observed in the spectrum (Fig. 3). These results corroborate with the findings of Aslibeiki *et al.* (2022) and confirm the formation of cubic $CoFe_2O_4$ particles.[45] Moreover, the FTIR spectrum of the blended Ni–Pd/C catalyst displayed a similar trend with a characteristic OH peak in the 3500 cm^{-1} region (Fig. 3). Additionally, the spectrum had distinct peaks at wavenumbers 1564 cm^{-1} and 1410 cm^{-1}, representing the stretching vibrations of C=C, while the slight protrusion around 1250 cm^{-1} results from the vibration of C–O bending.[46] The overlapping bands below 600 cm^{-1} are typical of metal–O vibrations, which could have appeared due to the presence of NiO.[47]

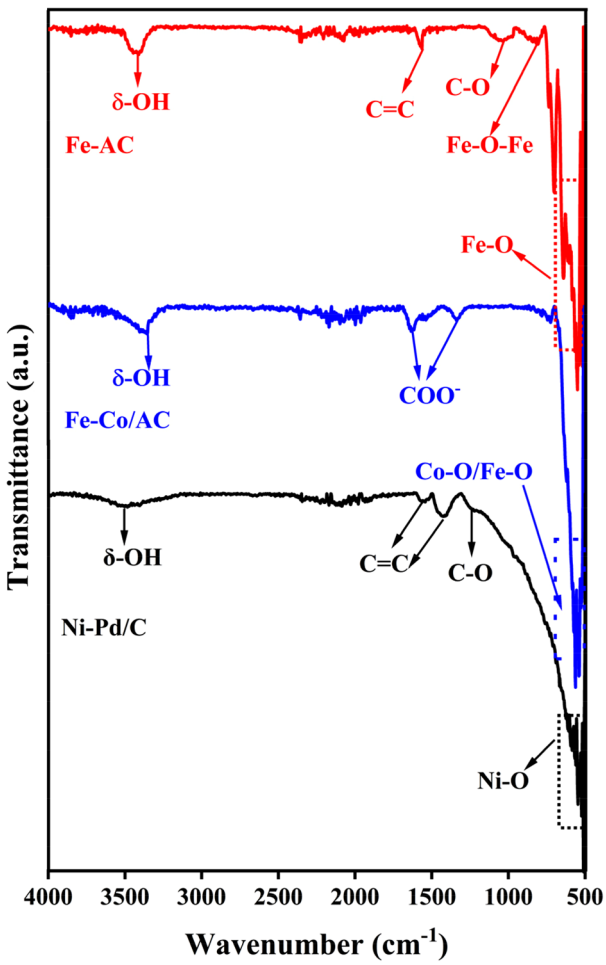

Fig. 3 The FTIR spectrum of AC-Fe (red); CoFe-AC (blue); and Ni–Pd/C (black) catalysts with the respective functional groups.

The shape, size, and arrangement pattern of the three BEF catalysts were analysed by FESEM. The FESEM image of heterogeneous AC-Fe and CoFe-AC catalysts indicated that all are well-structured and polydisperse, which was similar to observations in previous research.[48] Furthermore, the FESEM images depict that Ni, Pd, Co, and Fe metals are mostly in sphere-shaped or near-spherical shapes; however, AC is mostly in disorganised graphite form with a random amorphous and highly porous structure distribution (Fig. 4(A, C and E)). However, the structure of Ni–Pd/C perceived is in a more nano-colloidal form with an average size of 28 nm whereas CoAC-Fe and AC-Fe displayed an average size of 34 nm and 38 nm, respectively, as per calculation *via* J software.[49] Furthermore, the elemental distribution analysis of the FESEM-EDX spectrum showed a sharp peak of elements C, Fe, Co, Ni, and Pd, confirming their presence in the respective catalysts (Fig. 4(B, D and F)). Moreover, the weight % of C and Fe content was detected to be 35.85% and 63.94% whereas Co and Fe content was about 34.94% and 65.81% in the CoFe-Ac catalyst, respectively. Likewise, the two most dominant metals namely Ni and Pd, were detected in the Ni–Pd/C catalyst having a corresponding weight percentage of 38.43% and 61.57%, confirming the purity of the respective metals.

3.3 Quantification of H_2O_2 and identification of $^{\bullet}OH$ and ROS during the BEF reaction in the cathodic chamber of BEF-PMFCs

To elucidate the production of H_2O_2 in the BEF system, a quenching test was performed using 2-propanol as the $^{\bullet}OH$ scavenger. Firstly, 10 mg L^{-1} MB solution was poured into the cathodic chamber of all three test BEF-PMFCs and the control PMFC, and the change in the MB concentration was checked by taking aliquots at a suitable interval. For 2 h of retention time, almost complete decolourisation of MB (99.81 ± 0.10%)

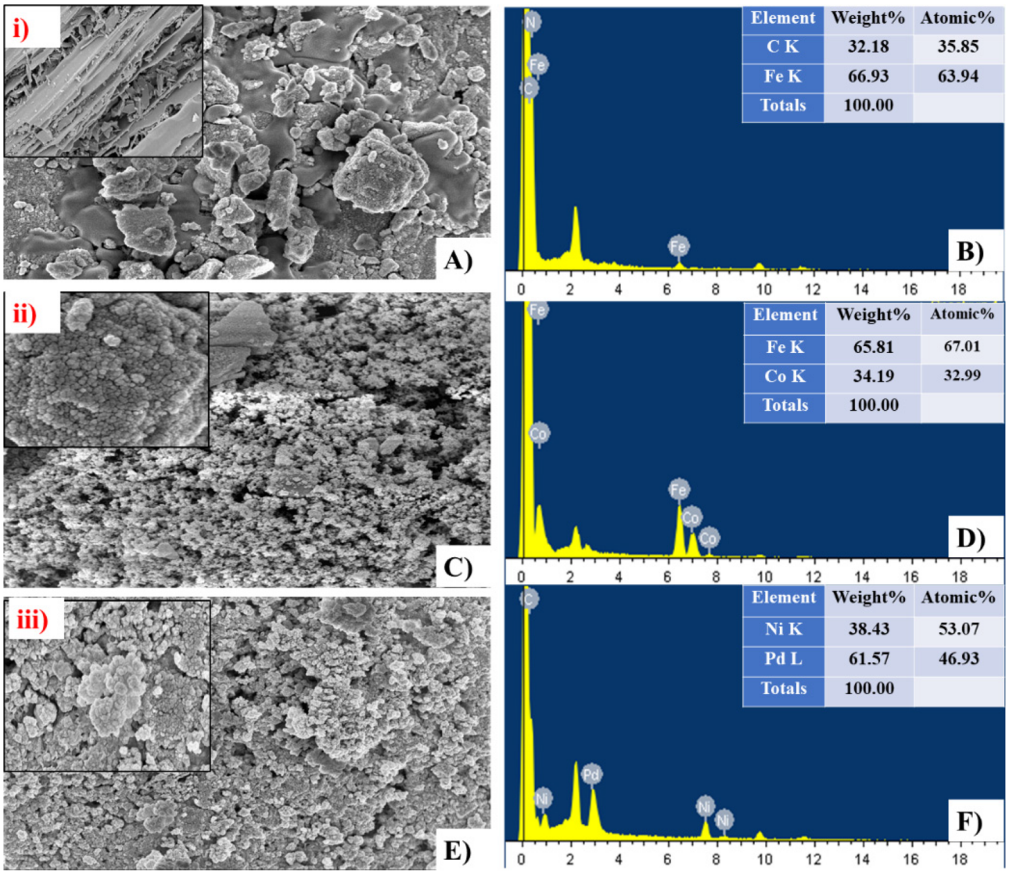

Fig. 4 The morphological characteristics of BEF catalysts (A) AC-Fe; inset (i) AC assembly; (B) spectrum analysis with elemental components of AC-Fe; (C) CoFe-AC with inset (ii) Co assembly; (D) spectrum analysis with elemental components of CoFe-AC; (E) Ni–Pd/C with inset (iii) Ni–Pd assembly; (F) spectrum analysis with elemental components of Ni–Pd/C.

was observed in the Ni–Pd/C catalysed BEF system while 92.89 ± 1.50% and 87.59 ± 2.10% removal was attained in the CoFe-AC and AC-Fe catalysed BEF systems, respectively (Fig. 5). Afterwards, the same experiment was repeated by adding 1 mM 2-propanol in the catholyte along with 10 mg L^{-1} MB in each of the BEF-PMFCs to scavenge *in situ* generated $^{\bullet}OH$. A substantial reduction in MB decolourisation was perceived for all three BEF systems. After 2 h of contact time, the degradation efficiency of MB reduced to 40.84% ± 1.10% for the Ni–Pd/C catalysed BEF, whereas for the CoFe-AC and AC-Fe assisted BEF systems, the value came down to 38.48 ± 2.70% and 36.51 ± 3.40%, respectively. These values resembled the MB removal efficiency of PMFC-C (34.21 ± 3.20%), which suggests that the degradation of MP was primarily due to the *in situ* generated $^{\bullet}OH$. The degradation efficiency of MB with and without the addition of 2-propanol is consistent with the findings of previous research.[50,51]

The formation of $^{\bullet}OH$ was further monitored *via* 5,5-dimethypylpyrroline-1-oxide (DMPO)-spin trapping EPR characterisation, which is regarded as a conclusive method for ROS identification in heterogeneous Fenton-based systems (Fig. 6). All three catalytic systems exhibited the distinct four-fold peak of complex adducts formed by the interaction of $^{\bullet}OH$ and DMPO.[52] Since the EPR trend for all catalysts was alike, the intensity of the peaks could be translated directly to the yield of $^{\bullet}OH$.[53] The peak of the DMPO adduct was more intense in the case Ni–Pd/C-Fe^{2+}, while the peak intensities for AC-Fe and CoFe-AC were more or less identical, suggesting that the $^{\bullet}OH$ yield was the highest for the Ni–Pd/C–Fe^{2+} catalysed system. This result corroborated with the findings of the quenching test and algae degradation result of the corresponding system.

3.4 Effect of different BEF catalysts for algal cell disruption, lipid yield, and chlorophyll removal

The estimation of algal cell death during BEF-assisted cell disruption was investigated using a hemocytometer to observe the cell mortality during Ni–Pd/C, CoFe-AC, and AC-Fe derived $^{\bullet}OH$-assisted hydrolysis. In this respect, algal cell death *vs.* time of incubation for different catalysts such as Ni–Pd/C, CoFe-AC, and AC-Fe are exemplified, where complete cell disruption was attained in the Ni–Pd/C-mediated Fenton oxidation process. Among the three BEF systems, the cell disruption for Ni–Pd/C catalysed-Fenton oxidation started within 1 h of incubation, whereas algal hydrolysis for the heterogeneous

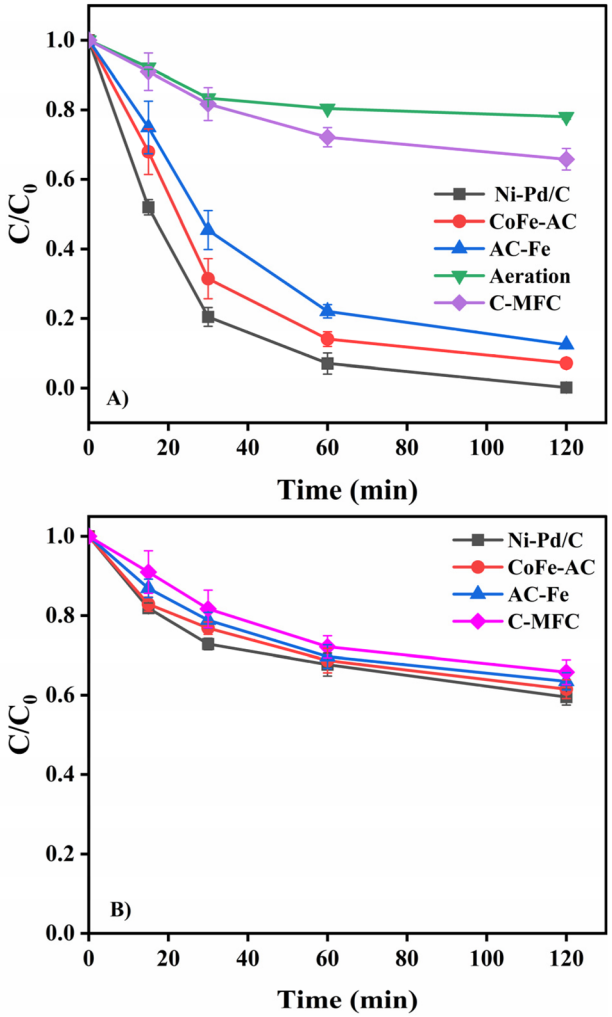

Fig. 5 Degradation of methylene blue (A) without, and (B) with the addition of 2-propanol.

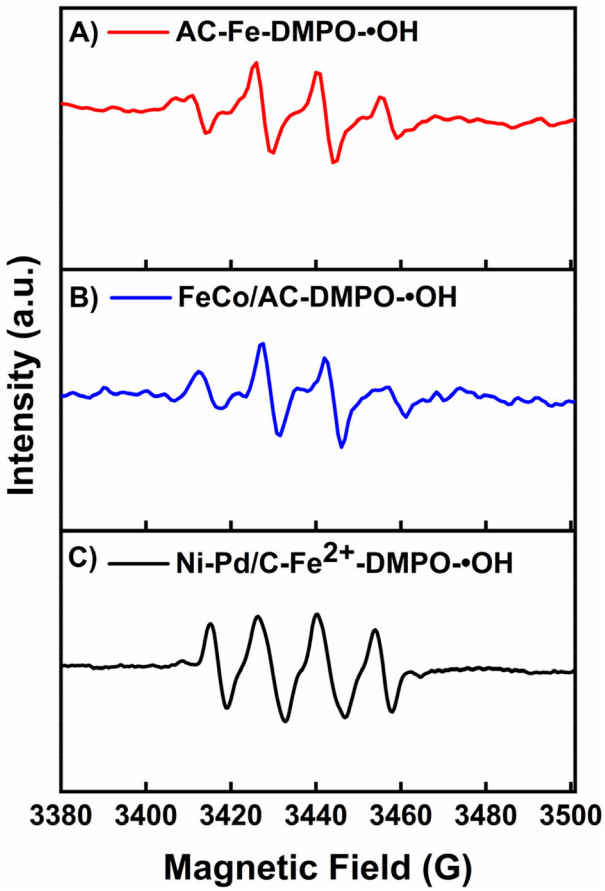

Fig. 6 The EPR spectra of (A) AC-Fe, (B) FeCo/AC, and (C) Ni–Pd/C-Fe^{2+} using DMPO as the trapping reagent.

CoFe-AC and AC-Fe-catalysed Fenton oxidation initiated after 2 h and 2.5 h of incubation, respectively (Fig. 7A). Thereafter, the algal cell death rate increased rapidly, attaining complete disruption within 6 h in the presence of the Ni–Pd/C catalyst coated cathode. The rate of cell death remained the same after 6 h, and nearly 99.8% of cell death was recorded, along with 38.5% lipid yield within 6 h of incubation.

In contrast to this, after 6 h of cell hydrolysation, the lipid molecule was degraded due to the presence of ROS, leading to the inferior recovery of lipid yield. Similarly, a total of 95% and 92% cell death was recorded during 6 h of incubation by employing CoFe-AC and AC-Fe as the catalyst in BEF-PMFC-T2 and BEF-PMFC-T3, respectively. In previous research, enzymatic cell disruption achieved 98.5% cell death after 16 h of prolonged incubation. Evidently, the algal cell wall was rapidly disintegrated by the BEF process, chiefly due to the generation of *in situ* $^{\bullet}OH$.[26] Moreover, Fe^{3+} ions form hydroxide species at neutral pH, which act as a coagulant. Therefore, leached or exhausted Fe^{3+} ions from CoFe-AC and AC-Fe might have assisted swifter settling of disrupted algal cell biomass during the BEF process. Hence, in comparison with traditional biological treatment techniques, the heterogeneous BEF process at circumneutral pH presents a quick and economical technique for lipid extraction.

In addition to excessive energy requirement, factitious pH regulation (pH 2.8–3.5) in the conventional electro-Fenton process is environmentally and economically disadvantageous.[54] In contrast, the self-driven BEF process can resolve this issue by using a cost-effective heterogeneous Fenton's catalyst, such CoFe-AC or AC-Fe, which has a broader working pH range. In this investigation, it was observed that homogeneous Ni–Pd/C catalyst is more active under acidic conditions, while the heterogeneous CoFe-AC and AC-Fe catalysts have shown excellent catalytic activity for *in situ* H_2O_2 and $^{\bullet}OH$ production in a wide pH range (3.0–9.0).[55] Moreover, lipids recovered from the heterogeneous catalyst-aided BEF reaction did not require further purification as the catalyst was not mixed with lipids during cell disruption. Although, homogeneous Fenton oxidation in the Ni–Pd/C and Fe^{2+} system can rapidly hydrolyse the algal cell, this requires further purification, which incurs an additional cost that hinders its commercial application. Another noteworthy challenge of using a

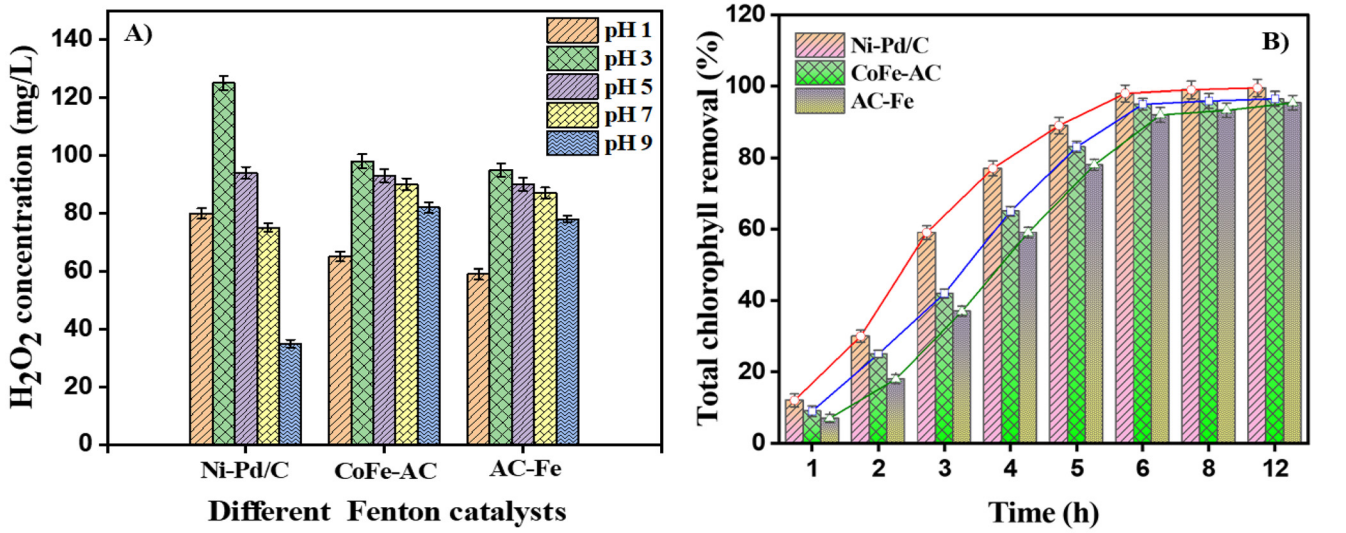

Fig. 7 (A) Variation of different H_2O_2 concentrations produced by employing different catalysts under the pH range from 1.0 to 9.0; (B) total chlorophyll removal (%) during the different time intervals.

homogeneous Fenton process is the non-recyclability of the catalyst, making it unsuitable for continuous systems. Clearly, better recyclability of catalysts in heterogeneous BEF processes is propitious for upscaling of this technology. Chlorophyll is the most troublesome impurity in biodiesel and must be eliminated to meet the quality criteria as a transportation fuel. Additionally, chlorophyll is often present in extracted lipids after solvent extraction due to its hydrophobicity.

This issue can be alleviated *via* the BEF process by rapid oxidation of large amounts of double carbon bonds present in chlorophyll. The concentrations of electrogenerated H_2O_2 at varied time intervals are in relation to the concentrations of total chlorophyll removal percentage as depicted in Fig. 7B. The chlorophyll removal percentage was significantly enhanced to 98.0% after 5 h of BEF reaction at pH 3.0. The initial concentration of chlorophyll was 55.3 μg mL^{-1}, and the Ni–Pd/C catalysed BEF reaction for 6 h removed 98% of chlorophyll. On the other hand, CoFe-AC and AC-Fe-aided BEF bleached 95%, and 92% of chlorophyll after 6 h of interaction. The green algal culture media was completely bleached from dark green to translucent after 24 h of $^{\bullet}OH$ oxidation. From the above findings, it can be concluded that acidic environment (pH = 3.0) is favourable for H_2O_2 electrogeneration (95–125 mg L^{-1}), while a contact time of 6 h is optimum for algal cell disruption for subsequent biodiesel recovery.

3.5 Optimisation of physicochemical factors for the recovery of lipids after algal cell disruption

Different parameters affecting the disruption of algal cell walls were assessed by optimising the electrolysis time, *in situ* H_2O_2 production, and catholyte pH based on the cell disruption efficiency and lipid recovery. The effect of the contact time variation, along with the concentration of electrogenerated H_2O_2 on the amount of extracted lipids by employing different Fenton's catalysts is shown in Fig. 8. The findings revealed that a maximum 39.2% (w/w) lipid was recovered from algae oxidised *via* the Ni–Pd/C and Fe^{2+} homogeneous system, which was 1.1-fold and 1.3-fold higher than heterogeneous CoFe-AC (37.5% w/w) and AC-Fe (30.9% w/w) mediated algal cell disruption, respectively. Subsequently, the lipid yield reduced to 17.5% w/w when algal biomass was not subjected to the BEF process. However, the amount of lipid yield was drastically reduced when the contact time was augmented beyond 12 h. This could be probably due to the oxidation of lipid molecules into lipid peroxide resulting from the prolonged attack of ROS.[14]

Furthermore, the efficiency of lipid extractability was also estimated to gauge the scalability of BEF-derived cell lysis process for practical implementation. A maximum of 95%,

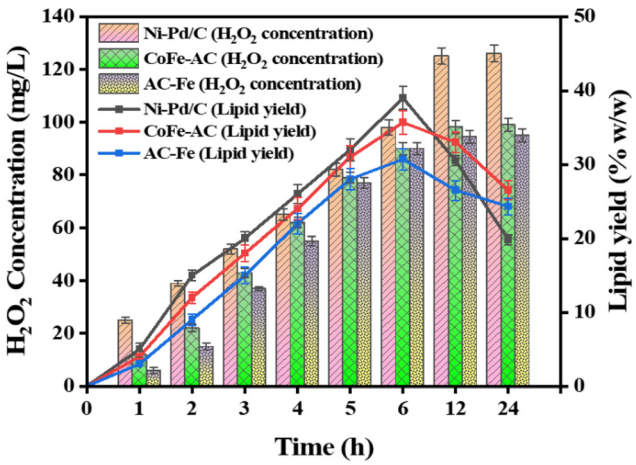

Fig. 8 Algal lipid yield obtained under different H_2O_2 concentrations produced by Ni–Pd/C, CoFe-AC, and AC-Fe catalysts.

91%, and 75% lipid extraction efficiency (based upon total lipid content) was achieved *via* Ni–Pd/C, CoFe-AC, and AC-Fe-assisted cell disruption, respectively, whereas only 60% lipid extraction efficiency was attained from the non-disruptive cell. In one investigation, an exceedingly high lipid extraction efficiency of 96% was achieved by inducing $SO^{4\bullet-}$ oxidation by adding 200 mg L^{-1} $FeCl_3$ to 540 mg L^{-1} $K_2S_2O_8$.[56] However, bio-based cell disruption, such as enzymatic cell lysis, obtained a highest of 85% lipids as per previous research.[26,57] Hence, the BEF process can be considered a rapid and highly efficient cell disruption technique over other biochemical approaches for lipid extraction from wet algal biomass.

3.6 Identification of lipid molecule by FTIR and FAME analysis with GC-MS

The FTIR analysis was conducted using a Bruker FTIR spectrometer, model number vertex 70 V, for determining the protuberant functional group present in algal lipids and de-oiled algal biomass (DAB). The spectrum was recorded in the range from 4000 to 400 cm^{-1} to recognise the functional group of algal carbohydrates, proteins and lipids.[58] In the crude lipid recovered *via* different catalyst-assisted BEF processes, sharp absorption peaks at 3200–3550 cm^{-1}, 2860–3220 cm^{-1}, and 1500–1980 cm^{-1} were observed in the FTIR spectrum due to the existence of OH and NH stretching, unsaturated hydrocarbon (=C–H stretching) and symmetric and asymmetric lipid acyl chains (–CH_2 and –CH_3), respectively. Additionally, ester and fatty acid ester group (C=O), alkane group (C=C stretch), alcohol groups (C–C(O)–C stretch), and alkene (C–H stretch) were also predominant in algal lipids with the occurrence of vibration at 1173–1480 cm^{-1}, 761–900 cm^{-1} and 460–590 cm^{-1} (Fig. 9A). Thus, the findings obtained from the FTIR spectrum proved that BEF-assisted algal lipid sample have C=C and –CH_2 symmetric and asymmetric stretching vibrations, which indicates the presence of lipids in a pure form.[59]

Besides, the de-fatted algal biomass after BEF-assisted cell disruption exhibits absorption spectra at 3200–3500 cm^{-1}, 1450–1680 cm^{-1}, and 947–1140 cm^{-1} for the existence of carboxylic acid, amide I and amide II bands, phosphoryl group and polysaccharides, respectively (Fig. 9B). In addition, a few minor adsorption bands ranging from 1600 to 1680 cm^{-1} were also observed in Fig. 9B, which might be the vibration peak of the associated phenolic groups in the vicinity. Hence, it is evidenced that the main components of the lipid deficient DAB were carbohydrates and proteins, indicating successful lipid extraction from wet algal biomass followed by BEF-assisted cell disruption.

3.7 Analysis of fatty acid profiles recovered after BEF-assisted cell disruption

Different fatty acid methyl esters (FAMEs) present in trans-esterified algal crude oil were detected *via* GC-MS by the developed method reported by Das *et al.* (2022).[60] The majority of the FAME components were observed from all the trans-esterified algal oil, where a higher number of methyl ester compounds were detected in the Ni–Pd/C and CoFe-AC-assisted lysed algal cells in comparison with the AC/Fe abetted disruptive cell (Table 1). Thus, the algal culture with BEF pre-treatment will aid in producing a higher number of FAMEs, which are the key ingredients for the synthesis of biodiesel from wet biomass.

The weight % of different fatty acids in algal lipids were quantified after transesterification of lipids extracted by employing BEF-based cell disruption under the optimal conditions in order to determine whether cell disruption treatments may have had an impact on the quality of the lipids. This experiment also attempted to confirm the potential of recovered lipids for the production of biodiesel.

The total fatty acids present in lipids extracted from intact biomass were identified as around 93% w/w, while FAMEs obtained from biomass disrupted with Ni–Pd/C, CoFe-AC, and

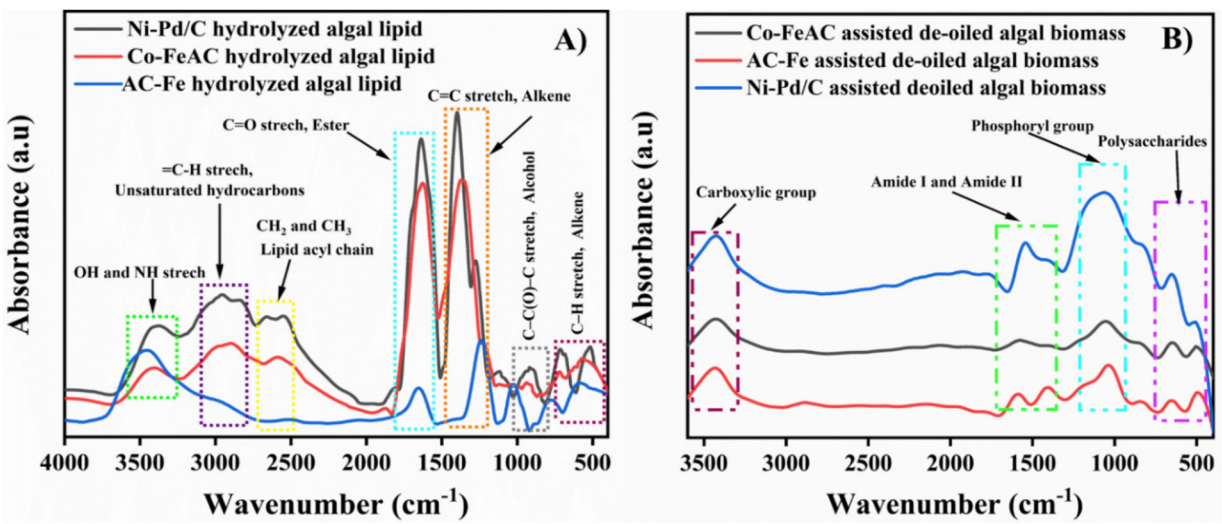

Fig. 9 (A) The FTIR spectra of algal lipid; and (B) lipid extracted de-oiled algal biomass.

Table 1 Identification of different fatty acid methyl esters from algal lipid hydrolysed by Fenton reaction through GC-MS

FAME components	Chemical formula	Retention time (min)	Ni–Pd/C	CoFe-AC	AC-Fe
Hexanoic acid, methyl ester	$C_7H_{14}O_2$	5.6	1.4	1.2	1.3
Caprylic acid, methyl ester	$C_9H_{18}O_2$	5.9	0.5	0.8	1.5
Pentanedioic acid, 2,4-dimethyl ester	$C_9H_{16}O_4$	6.3	1.3	1.2	ND
Undecylic acid, methyl ester	$C_{11}H_{22}O_2$	6.5	3.2	3.8	4.3
Dodecanoic acid methyl ester	$C_{13}H_{26}O_2$	6.7	2.2	2.1	1.2
Undecanoic acid, 10-methyl, methyl ester	$C_{13}H_{26}O_2$	6.9	4.3	4.2	4.9
Tridecanoic acid, 12-methyl, methyl ester	$C_{14}H_{28}O_2$	7.3	8.5	7.7	6.5
Tetradecanoic acid, 12-methyl ester	$C_{16}H_{32}O_2$	8.5	9.5	9.2	8.8
7,10-Hexadecadienoic acid, methyl ester	$C_{17}H_{30}O_2$	9.2	1.2	ND	ND
Methyl palmitoleate	$C_{17}H_{32}O_2$	9.5	2.8	4.4	5.8
Palmitic acid, methyl ester	$C_{17}H_{34}O_2$	10.0	17.3	15.5	12.8
4-Ethyl benzoic acid, 6-ethyl-3-octyl ester	$C_{17}H_{26}O_2$	10.5	1.9	3.6	ND
Heptadecanoic acid, methyl ester	$C_{18}H_{36}O_2$	11.2	0.8	0.6	0.5
Oleic acid methyl ester	$C_{19}H_{36}O_2$	12.6	8.3	7.4	5.1
12,15-Octadecadienoic acid, methyl ester	$C_{19}H_{30}O_2$	16.0	5.1	4.5	3.9
Linolenic acid methyl ester	$C_{19}H_{32}O_2$	18.2	2.1	2.3	2.8
Linoleic acid methyl ester	$C_{19}H_{34}O_2$	20.5	9.5	8.3	8.2
Stearic acid methyl ester	$C_{19}H_{38}O_2$	21.4	4.2	4.8	5.8
Arachidic acid methyl ester	$C_{21}H_{42}O_2$	22.5	2.1	4.0	6.1
Docosahexaenoic acid methyl ester	$C_{23}H_{34}O_2$	23.2	2.9	2.4	ND
13,16-Docosadienoic acid methyl ester	$C_{23}H_{42}O_2$	25.4	0.8	0.9	0.2
Tricosanoic acid methyl ester	$C_{24}H_{48}O$	28.5	1.5	ND	1.1
Tetracosanoic acid, methyl ester	$C_{25}H_{50}O_2$	29.8	3.2	3.1	2.7
Others			3.5	8.0	16.5

ND: not detected; all FAME concentrations (mg L^{-1}) are estimated based upon Supelco® 37-lipid component standards.

AC-Fe were recovered around 98% w/w, 96% w/w, and 95% w/w, respectively. Moreover, the total saturated fatty acid (SFA), monounsaturated fatty acid (MUFA), and polyunsaturated fatty acid (PUFA) were compared and the FAME profiles in terms of the weight % of each fatty acid relative to the total number of FAMEs were analysed.

The FAMEs recovered from lipids extracted from intact biomass had higher concentrations of unsaturated fatty acids, which accounted for about 45.5% w/w PUFA (among them 30.0% total linolenic acid (both α and γ)), and 26.7% w/w MUFA were identified. In contrast, a low content of the most important fatty acids for making biodiesel, such as total SFA (20.8% w/w) and MUFA (26.7% w/w) fatty acids, was observed in non-disrupted biomass. A similar type of FAME profile was obtained from non-disrupted wet algal biomass in previous investigations.[15]

Therefore, the biodiesel produced from biomass without subjecting to Fenton treatment is more unstable than that produced from Fenton-treated biomass due to the aforementioned features. Since untreated biomass-derived FAMEs have a higher degree of unsaturation, thereby the recovered biodiesel is more susceptible to oxidation when exposed to air, light, heat, trace metals, and other hostile conditions.[61] Hence, biodiesel extracted from non-disrupted algal biomass requires hydrolysation pre-treatment to enhance the quality of biodiesel. Conversely, when the cell disruption pre-treatment was carried out by the BEF process, the above-mentioned downsides were greatly diminished, which was further proved by FAME analysis of disrupted biomass (Table 2).

In detail, a total of 4.2%, 6.5%, and 7.0% w/w linolenic acid ($C_{18:3n3}$ and $C_{18:3n6}$) was obtained prior to cell disruption by Ni–Pd/C, CoFe-AC, and AC-Fe-catalysed BEF process, which was *ca.* 7.1-fold, 4.6-fold and 4.3-folds lower than no prior treatment (30.0% w/w). Concurrently, a significant increase in

Table 2 Fatty acid composition (% of total fatty acid) obtained from different BEF treatments

Lipid and fatty acid component (% w/w)	Wet lipid extraction without cell disruption	BEF-Ni–Pd/C	BEF-CoFe-AC	BEF-AC-Fe
$C_{10:0}$	0.40 ± 0.08	0.80 ± 0.09	0.60 ± 0.08	0.50 ± 0.05
$C_{11:0}$	1.50 ± 0.10	0.30 ± 0.12	0.20 ± 0.09	0.20 ± 0.08
$C_{12:0}$	1.70 ± 0.13	2.00 ± 0.15	1.40 ± 0.18	1.50 ± 0.11
$C_{13:0}$	0.20 ± 0.01	0.30 ± 0.02	0.40 ± 0.04	0.60 ± 0.01
$C_{14:0}$	1.00 ± 0.01	1.20 ± 0.09	1.00 ± 0.11	1.40 ± 0.09
$C_{15:0}$	1.20 ± 0.09	0.20 ± 0.01	0.10 ± 0.01	Not detected
$C_{16:0}$	8.20 ± 1.15	30.60 ± 1.81	28.20 ± 1.22	25.50 ± 1.02
$C_{17:0}$	1.10 ± 0.01	0.50 ± 0.02	0.60± 0.02	0.70 ± 0.02
$C_{18:0}$	1.20 ± 0.11	2.50 ± 0.06	2.00 ± 0.04	2.60 ± 0.08
$C_{20:0}$	4.00 ± 0.23	4.50 ± 0.21	4.30 ± 0.21	4.60 ± 0.11
$C_{23:0}$	0.30 ± 0.01	0.50 ± 0.11	Not detected	0.40 ± 0.09
∑SFA (% of total fatty acid)	20.80 ± 1.89	42.50 ± 2.80	38.80 ± 2.01	36.90 ± 1.51
$C_{14:1}$	3.70 ± 1.01	2.60 ± 1.11	3.80 ± 0.09	4.80 ± 0.09
$C_{15:1}$	2.10 ± 0.19	2.90 ± 0.62	2.50 ± 0.06	2.90 ± 0.06
$C_{16:1}$	5.50 ± 0.21	4.80 ± 0.15	4.70 ± 0.02	4.20 ± 0.05
$C_{17:1}$	1.40 ± 0.09	0.90 ± 0.85	1.60 ± 0.03	1.80 ± 0.02
$C_{18:1n9}$	6.80 ± 0.93	11.80 ± 1.10	10.50 ± 0.06	9.80 ± 0.03
$C_{20:1}$	3.00 ± 0.14	6.70 ± 0.25	5.90 ± 0.09	4.70 ± 0.01
$C_{22:1n9}$	4.20 ± 0.37	3.80 ± 0.17	3.70 ± 0.01	3.60 ± 0.02
∑MUFA (% of total fatty acid)	26.70 ± 2.19	35.50 ± 3.95	34.70± 3.87	33.80 ± 2.72
$C_{18:2n6t}$	4.50 ± 1.89	8.60 ± 0.02	3.80 ± 0.02	4.70 ± 0.02
$C_{18:2n6c}$	4.40 ± 1.89	8.40 ± 0.01	6.90 ± 0.07	6.20 ± 0.04
$C_{18:3n3}$	15.60 ± 1.89	2.10 ± 0.01	3.20 ± 0.08	3.40 ± 0.03
$C_{18:3n6}$	14.40 ± 1.89	2.10 ± 0.02	3.30 ± 0.03	3.60 ± 0.01
$C_{20:5n3}$	6.60 ± 1.89	0.40 ± 0.03	0.80 ± 0.02	0.90 ± 0.01
∑PUFA (% of total fatty acid)	45.50 ± 1.89	21.60 ± 1.11	22.50 ± 1.29	23.80 ± 1.83

SFA: saturated fatty acid; MUFA: monounsaturated fatty acid; PUFA: polyunsaturated fatty acid; BEF: bio-electro-Fenton.

the amount of palmitic acid (C16 : 0) was found when disruption was carried out using Ni–Pd/C (30.6% w/w), CoFe-AC (28.3%) and AC-Fe (25.5% w/w) catalysts, compared to the respective fatty acid recovered from undisrupted algal biomass (8.2% w/w). Additionally, linoleic acid, which is useful for making biodiesel, was also enhanced by BEF-assisted cell disruption in comparison with no prior treatment. From the FAME analysis, it was observed that a total 17.0% w/w *cis* and *trans* linoleic acid (C18:2n6c and C18:2n6t) was found after Ni–Pd/C-mediated BEF treatment, whereas only 8.9% w/w total linoleic acid was obtained from non-disrupted cell. Besides, the accumulated weight % of total SFA for cell disruption with BEF reaction was 42.5% w/w (Ni–Pd/C), 38.8% w/w (CoFe-AC), and 35.9% w/w (AC-Fe), and these values were noticeably higher than the equivalent ones observed without any treatment (20.8% w/w). Also, the cumulative percentage of MUFA was obtained as 35.5% w/w, 34.7% w/w, and 33.8% w/w for the Ni–Pd/C, CoFe-AC, and AC-Fe assisted BEF-disrupted microalgae, respectively, compared to non-disrupted algae (Table 2). This might be due to the degradation of more PUFA by the ROS generated during the BEF process, which was further evidenced by the significantly lower PUFA fractions in the BEF systems as compared to algal lipids recovered without any treatment. In conclusion, the BEF-based disruptive pre-treatment by different homogeneous and heterogeneous catalysts causes the concentration of desired fatty acids to increase while simultaneously decreasing the concentration of the undesirable ones and thereby resulting in the high quality of biodiesel in addition to achieving greater lipid yields.

3.8 Estimation of biodiesel quality parameters of BEF-assisted algal lipids

Generally, microalgae produce a variety of lipid moieties, including phospholipids, glycolipids, mono-, di-, and triglycerides, and only triglycerides are easily converted to biodiesel by the process of acid/base transesterification. However, the concentration of triglycerides is varied by the growth conditions, and the lipid extraction process. Algal cell disruption *via* $^{\bullet}OH$ causes significant changes in fatty acid composition that imparts conducive fuel properties. Therefore, different biodiesel quality parameters such as kinematic viscosity (ν), oxidative stability (OS), gross calorific value (GCV), iodine value (IV), saponification value (SV), degree of unsaturation (DU), and cetane number (CN) of the trans-esterified algal oil treated in the BEF process was estimated. Moreover, all the estimated values were further compared to biodiesel standards ASTM D6751-08 and EN 14214. One of the key characteristics that affects the combustion of any fuel is kinematic viscosity. When the chain length of the fatty acid or alcohol moiety in a FAME or an aliphatic hydrocarbon increases, the viscosity also increases, and it is often higher than that of petroleum diesel. The kinematic viscosity at 40 °C for biodiesel converted from algal lipid obtained *via* all three BEF systems was estimated to be 4.0, 4.1 and 4.3 $mm^2\ s^{-1}$, respectively, which is within the range specified by ASTM D6751 (1.9–6.0 $mm^2\ s^{-1}$) and EN 14214 (3.5–5.0 $mm^2\ s^{-1}$).[62] Moreover, the GCV epitomises the higher value of the heat of combustion, *i.e.*, the amount of chemical energy produced during the combustion of a unit mass of fuel. The typical GCV of microalgal biodiesel has been reported to be ~41 MJ kg^{-1}, and all derived GCVs of the algal lipid extracted after BEF treatment met this EN 14214 standard and were found to be similar to values reported by Sandani *et al.* (2022).[14]

The SV of an oil signifies the quantity of KOH required to neutralise the fatty acids. In line with this, biodiesel with FAMEs that have a lower average chain length results in a higher SV. However, an oil with a higher saponification value is more suitable for soap-making rather than the production of biodiesel. In this investigation, the SV value of BEF-Ni–Pd/C treated algal oil (190.4 mg of KOH) was 1.1 times lower than without pre-treated algal oil (214.4 mg of KOH), which further proves the suitability for decent algal biodiesel production (recommended value < 500). According to ASTM standard, the minimum required CN is 47, and it is usually linked with a higher degree of unsaturation. In this investigation, the CN of biodiesel produced from lipids obtained from the BEF-assisted cell disruption techniques fulfilled the standards mentioned in ASTM D6751-12 and EN 14214:2012 (Table 3). The CN of biodiesel produced from lipids extracted using the BEF process was marginally greater than lipids acquired from untreated biomass.

Another crucial factor that affects the stability of biodiesel during long-term storage is OS. The number of double bonds present in the algal fatty acids are assessed using the IV of bio-

Table 3 Quality parameters of biodiesel produced from algal lipids extracted by the BEF process

Biodiesel property	Without cell disruption	BEF-Ni–Pd/C	BEF-CoFe-AC	BEF-AC-Fe	European (EN 14214) biodiesel	ASTM D6751-12
Kinematic viscosity ($mm^2\ s^{-1}$)	4.5	4.0	4.1	4.3	3.5–5.0	1.9–6.0
Oxidative stability (h)	8.0	8.5	8.3	8.2	≥8	—
Calorific value (MJ kg^{-1})	40.1	40.9	40.7	40.6	~41	≤45
Saponification value (mg of KOH)	214.4	190.4	195.4	198.8	<500	<500
Cetane number (min)	50.2	48.2	48.5	48.0	45–55	—
Iodine value (g I_2/100 g of lipid)	101.6	112.2	108.4	106.4	<130	100–120
Degree of unsaturation (% w)	93.8	82.3	82.8	83.2	—	—

BEF: bio-electro-Fenton.

diesel, which aids in calculating the OS of biodiesel. In the present investigation, oil recovered from Ni–Pd/C and Fe^{2+}-treated algal cells had a DU of 82.3%, which was 14% lower than that recovered from untreated algal biomass and thus, demonstrating an adequate OS value. In addition, the BEF-treatment also reduced unsaturation in fatty acids, causing a lowering of IV values that indicates better fuel quality. A maximum IV value of 120 g I_2/100 g is acceptable in determining the fuel quality as per standard, which was complied with by the oil extracted by the BEF process (Table 3). Similarly, biodiesel made from algal lipids extracted using the BEF process showed considerably higher OS and achieved full compliance with ASTM D6751-12 (≥8) relative to the lipids obtained through untreated wet biomass. This higher OS quality might be reflected by the reduced percentage of PUFA in the lipids produced *via* the BEF process. In summary, BEF-assisted cell disruption generated a higher lipid yield while maintaining the quality of biodiesel as specified by ASTM D6751-12 and EN 14214:2012. Hence, BEF-assisted algal cell disruption can be a promising green strategy for lipid extraction from wet algal biomass over conventional physicochemical approaches.

3.9 Electrochemical analysis of BEF-assisted PMFC

The electrical performance of BEF-PMFC-T1, BEF-PMFC-T2, and BEF-PMFC-T3 fabricated with the carbon felt cathode coated with Ni–Pd/C, CoFe-AC, and AC-Fe as cathode catalysts, respectively, was explored and compared with that of control PMFC. Firstly, the CV analysis of all three catalysts was performed to evaluate the ORR properties for their applicability as the cathode catalyst in PMFC. The representative CV profiles are depicted in Fig. 10A, where the maximum reduction peak with current density of −64.2 mA m^{-2} was observed at −0.35 V *vs.* Ag/AgCl for Ni–Pd/C catalyst. This observation clearly recommends that Ni–Pd/C catalyst is more active towards the ORR. In comparison, the CV profile of CoFe-AC exhibits the highest current density peak of −44.1 mA m^{-2} at −0.69 V (V *vs.* Ag/AgCl), which was 2.9-fold higher than that of AC-Fe (−15.0 mA m^{-2} at a potential of −0.72 V).

The higher electro-catalytic activity of CoFe-AC towards the ORR can be attributed to the higher content of surface functional groups due to the presence of transition metals, which is comparable with previously reported literature under identi-

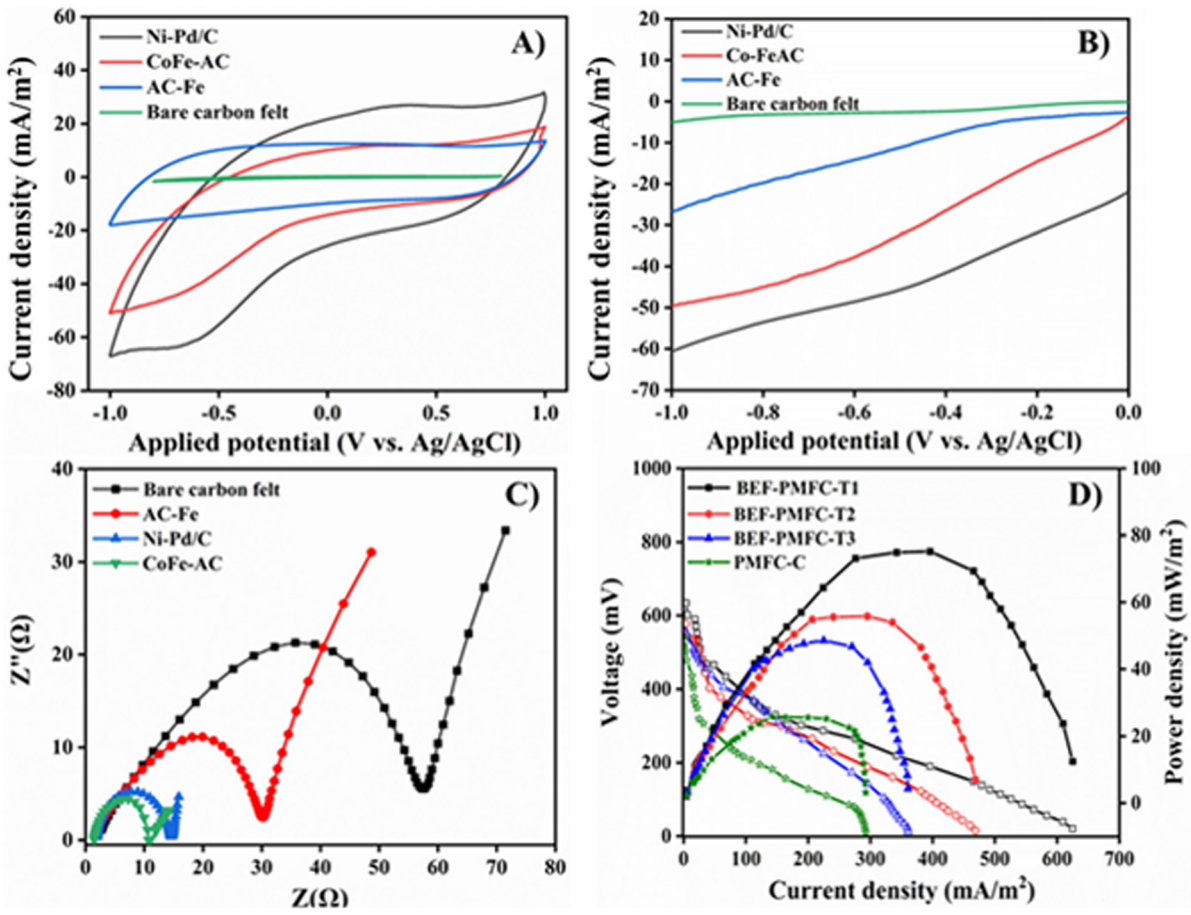

Fig. 10 (A) The CV and (B) LSV analysis of Ni–Pd/C, CoFe-AC, and AC-Fe catalysts in comparison with bare carbon felt; (C) the Nyquist plots of bare carbon felt and different catalyst-coated electrodes during the EIS test; and (D) polarisation curves of different catalyst-coated BEF-PMFC.

cal electro-catalytic conditions. Correspondingly, the highest oxidation peak at 26.9 mA m^{-2} at 0.35 V was achieved by the Ni–Pd/C catalyst, which was also *ca.* 2.2-times and 2.4-times higher in comparison with that of CoFe-AC and AC-Fe, respectively. Moreover, the CV analysis of bare carbon felt devoid of any catalyst generated a very lower reduction and oxidation current (not detectable) in comparison with other three cathode catalysts.

Analogously, BEF-PMFC-T1 generated a maximum current density of 625.2 mA m^{-2}, which was 1.3, 1.7 and 2.1-times higher than that by BEF-PMFC-T2 (468.7 mA m^{-2}), BEF-PMFC-T3 (360.5 mA m^{-2}) and PMFC-C (292.4 mA m^{-2}), respectively. According to the LSV plot, the reduction peak of Ni–Pd/C catalyst (−60 mA m^{-2}), was more distinct than that of CoFe-AC and AC-Fe, suggesting that the Ni–Pd/C catalyst was more adept at accelerating the ORR than the other two cathode catalysts (Fig. 10B). Further, the absence of any perceivable peak in the CV plot of bare carbon felt confirmed that the addition of Fenton catalysts amplified the ORR activity resulting in distinct reduction current peaks. Intriguingly, the CoFe-AC composite showed 2.0-times higher reduction peak (−50 mA m^{-2}) than AC-Fe, thus signifying its suitability as an efficient cathode catalyst.

The OV and OCV of all PMFCs were periodically monitored, and BEF-PMFC-T1 attained the highest OV of 162.8 ± 10.5 mV and OCV of 658.5 mV ± 52.3, which were 2.0-fold and 1.2-fold greater than that of PMFC-C (OV: 81.6 ± 9.2; OCV: 550.8 ± 35.6), respectively (Table S2†). Congruently, the maximum 74.5 mW m^{-2} power density was attained by BEF-PMFC-T1, which was also *ca.* 1.3-times, 1.5-times, and 2.8-times greater in comparison with that of BEF-PMFC-T2 (56.8 mW m^{-2}), BEF-PMFC-T3 (48.6 mW m^{-2}) and PMFC-C (25.8 mW m^{-2}), respectively (Fig. 10C). This could be ascribed to the fact that the ORR activity in the cathodic chamber of the BEF-PMFC-T3 and BEF-PMFC-T2 were significantly catalysed by the addition of Ni–Pd/C and CoFe-AC, respectively. Furthermore, the Ni–Pd/C coated electrode showed the least charge transfer resistance (R_{ct}) of 9 Ω as computed from the EIS plot, which was 6.6-fold lower than that of bare carbon felt (60 Ω) (Fig. 10D).

The R_{ct} value is a critical determinant for the ORR, with a lower value of R_{ct} typically indicating faster electron transfer ability and high electrical conductivity. Certainly, the extremely low R_{ct} value of Ni–Pd/C confirms the superiority of the Ni–Pd/C catalyst in accentuating cathode activity over the other two catalysts. Nevertheless, the R_{ct} of CoFe-AC (14 Ω) coated electrode was only slightly higher than that of the Ni–Pd/C catalysed system. In fact, the potency of CoFe-AC in accentuating the ORR kinetics was cemented by R_{ct} values that were 2.2 and 4.3 times lower than those of AC-Fe (30 Ω) and bare carbon felt, respectively. Overall, the material and electrochemical characterisation confirmed that in addition to being a remarkable Fenton's catalyst, CoFe-AC is also a promising electrocatalyst for the ORR with sufficiently low onset potential in BEF-PMFC and a cost-effective substitute for the expensive Ni–Pd/C catalyst.

3.10 Wastewater treatment and energy recovery from BEF-aided PMFCs

The efficacy of wastewater treatment in terms of COD removal efficiency and simultaneous CE of all BEF-PMFCs were examined to elucidate the effects of utilising Ni–Pd/C, CoFe-AC, and AC-Fe as cathode catalysts. The CE of BEF-PMFC-T1 (24.7%), BEF-PMFC-T2 (22.3%), and BEF-PMFC-T3 (20.5%) was 76.4%, 59.2% and 46.4% higher in comparison with that of control PMFC (14.0%) (Table S2†). A similar trend was observed in COD removal efficiency of all BEF-PMFCs implying that the bioelectrochemical activity of *exo*-electrogens was also enhanced due to the presence of the ORR active Ni–Pd/C catalyst, resulting in higher consumption of organic matter as a substrate present in synthetic wastewater.[63] As a result, BEF-PMFC-T1 (89.2%), BEF-PMFC-T2 (85.5%), and BEF-PMFC-T3 (81.2%) demonstrated a higher COD removal efficiency in comparison with PMFC-C (72.3%), respectively.

A comparative result of performance efficiency is also listed in Table S3† in support of the premise that BEF oxidation processes are substantially more efficient than other physicochemical techniques. These findings ascertained that the overall performance of CoFe-AC was on par with that obtained using Ni–Pd/C as cathode catalysts. Hence, it is established that CoFe-AC composite can accelerate the ORR and catalyse Fenton's oxidation in BEF-PMFCs, presenting a greener route for algal biodiesel production. Corroborative findings from earlier research support the thought that heterogeneous Fenton's catalyst CoFe-AC and Ni–Fe are also promising cathode catalysts that ameliorate the ORR with sufficiently low onset potential in MFC.[64–66] However, this tenet needs to be backed through further investigations and techno-economic analysis of actual prototypes, preferably at real-scale usage.

4. Conclusions

Drawing energy from renewable sources can alleviate the ecological damage potential of Fenton oxidation. In this sense, the BEF process is gaining wide acceptance as a plausible substitute for offsetting the environmental impacts of traditional electrochemical processes. The BEF reaction employing Ni–Pd/C and homogeneous Fe^{2+} achieved a maximum lipid yield of 39.2% w/w from wet algal biomass after 6 h of reaction at pH 3.0, which was comparatively higher than that obtained without treatment. In addition to this, the grade of biodiesel synthesised from lipids extracted *via* BEF met all standards specified by ASTM D6751-12. Furthermore, the BEF-PMFC cathode coated with Ni–Pd/C generated a maximum of 74.5 mW m^{-2} power density, which was *ca.* 2.8 times higher compared to PMFC-C. Nevertheless, further improvements are still required to ameliorate the lipid yield, and techno-economic and environmental impact assessment should be performed prior to the large-scale implementation of this process. Hence, considering the encouraging outcomes of this investigation, the BEF-mediated cell lysis process for lipid extraction

can rekindle sustainable biodiesel production from algal feedstock.

Author contributions

Swati Das – conceptualization; visualization; validation; writing – original draft; writing – review and editing; software support; formal analysis; investigation. Rishabh Raj – visualization; methodology; validation; writing – original draft; writing – review; software support. M. M. Ghangrekar – resources; funding acquisition; supervision; project administration; writing – review and editing.

Data availability

The corresponding author will provide access to all the data used to support this research upon receiving an adequate request.

Conflicts of interest

The authors certify that none of their known financial conflicts of interest or close personal ties might have appeared to have influenced the research presented in this investigation.

Acknowledgements

The funding received from the Ministry of New and Renewable Energy, Government of India (IIT/SRIC/R/REF/2018/101) is duly acknowledged.

References

1 S. Das, R. Raj, S. Das and M. M. Ghangrekar, *Environ. Sci. Pollut. Res.*, 2022, 1–18.
2 K. Sonu, Z. Syed and M. Sogani, *J. Sci. Ind. Res.*, 2019, **78**, 555–557.
3 M. Kumar, X. Xiong, Y. Sun, I. K. Yu, D. C. Tsang, D. Hou, J. Gupta, T. Bhaskar and A. Pandey, *Adv. Sustainable Syst.*, 2020, **4**, 1900149.
4 A. Ahirwar, S. Das, S. Das, Y.-H. Yang, S. K. Bhatia, V. Vinayak and M. M. Ghangrekar, *Algal Res.*, 2023, 102973.
5 A. Khandelwal, M. Chhabra and P. Yadav, *Bioresour. Technol.*, 2020, **310**, 123418.
6 H. Chang, H. Feng, R. Wang, X. Zhang, J. Wang, C. Li, Y. Zhang, L. Li and S.-H. Ho, *Water Res.*, 2023, **231**, 119578.
7 A. Coşgun, M. E. Günay and R. Yildirim, *Green Chem.*, 2023, **25**, 3354–3373.
8 P. M. Foley, E. S. Beach and J. B. Zimmerman, *Green Chem.*, 2011, **13**, 1399–1405.
9 M. H. Kamani, I. Eş, J. M. Lorenzo, F. Remize, E. Roselló-Soto, F. J. Barba, J. Clark and A. M. Khaneghah, *Green Chem.*, 2019, **21**, 3213–3231.
10 N. Wang, S. Ma, P. Zuo, J. Duan and B. Hou, *Adv. Sci.*, 2021, **8**, 2100076.
11 G.-L. Chai, Z. Hou, T. Ikeda and K. Terakura, *J. Phys. Chem. C*, 2017, **121**, 14524–14533.
12 J. Feng and Y. Zhang, *New J. Chem.*, 2020, **44**, 16584–16593.
13 S. Das, A. Mishra and M. Ghangrekar, *J. Hazard., Toxic Radioact. Waste*, 2020, **24**, 06020001.
14 W. P. Sandani, M. Premaratne, T. U. Ariyadasa and J. K. Premachandra, *Bioresour. Technol.*, 2022, **343**, 126110.
15 A. Steriti, R. Rossi, A. Concas and G. Cao, *Bioresour. Technol.*, 2014, **164**, 70–77.
16 R. Daghrir, P. Drogui, N. Delegan and M. A. El Khakani, *Sci. Total Environ.*, 2014, **466**, 300–305.
17 N. Zhang, J. Bu, Y. Meng, J. Wan, L. Yuan and X. Peng, *Appl. Organomet. Chem.*, 2020, **34**, e5612.
18 S. Das, S. Das and M. Ghangrekar, *Bioresour. Technol.*, 2019, **294**, 122138.
19 Q. Zhang, X. Tan, N. M. Bedford, Z. Han, L. Thomsen, S. Smith, R. Amal and X. Lu, *Nat. Commun.*, 2020, **11**, 4181.
20 Z. Wang, L. Pi, J. Cui, X. Zhang, Y. Liu, D. Tang, H. Zhu and X. Mao, *Sep. Purif. Technol.*, 2021, **255**, 117731.
21 P. Bhuyar, M. H. A. Rahim, S. Sundararaju, R. Ramaraj, G. P. Maniam and N. Govindan, *Beni-Suef Univ. J. Basic Appl. Sci.*, 2020, **9**, 1–15.
22 E. Graf and J. T. Penniston, *Clin. Chem.*, 1980, **26**, 658–660.
23 S. K. Prajapati, A. Bhattacharya, A. Malik and V. Vijay, *Algal Res.*, 2015, **8**, 8–14.
24 J.-Y. Park, S.-A. Choi, M.-J. Jeong, B. Nam, Y.-K. Oh and J.-S. Lee, *Bioresour. Technol.*, 2014, **162**, 379–383.
25 B. Cheirsilp and S. Torpee, *Bioresour. Technol.*, 2012, **110**, 510–516.
26 S. Das, S. Das and M. Ghangrekar, *Bioresour. Technol.*, 2022, **363**, 127924.
27 M. Premaratne, V. C. Liyanaarachchi, G. K. S. H. Nishshanka, P. Nimarshana and T. U. Ariyadasa, *J. Environ. Chem. Eng.*, 2021, **9**, 105765.
28 A. P. H. Association, Standard methods for the examination of water and wastewater, *Am. Public Health Assoc.*, 1926.
29 S. Das, R. Raj, S. Das and M. M. Ghangrekar, *Front. Sustain.*, 2021, **2**, 104.
30 P. W. Gerbens-Leenes, M. M. Mekonnen and A. Y. Hoekstra, *Water Resour. Ind.*, 2013, **1**, 25–36.
31 Y. Li, C. Zhu, T. Lu, Z. Guo, D. Zhang, J. Ma and S. Zhu, *Carbon*, 2013, **52**, 565–573.
32 J.-Y. Lu, Y.-R. Yuan, X. Hu, W.-J. Liu, C.-X. Li, H.-Q. Liu and W.-W. Li, *Ind. Eng. Chem. Res.*, 2020, **59**, 1800–1808.
33 M. Sun, X. Han and S. Chen, *Mater. Sci. Semicond. Process.*, 2019, **91**, 367–376.
34 K. Chakrapani, G. Bendt, H. Hajiyani, I. Schwarzrock, T. Lunkenbein, S. Salamon, J. Landers, H. Wende, R. Schlögl and R. Pentcheva, *ChemCatChem*, 2017, **9**, 2988–2995.

35 S. Swathi, R. Yuvakkumar, P. S. Kumar, G. Ravi and D. Velauthapillai, *Chemosphere*, 2021, **281**, 130903.
36 M. Serwar, U. A. Rana, H. M. Siddiqi, S. U.-D. Khan, F. A. A. Ali, A. Al-Fatesh, A. Adomkevicius, J. A. Coca-Clemente, L. Cabo-Fernandez and F. Braga, *RSC Adv.*, 2017, **7**, 54626–54637.
37 A. E. Galetti, M. N. Barroso, A. Monzón and M. C. Abello, *Mater. Res.*, 2015, **18**, 1278–1283.
38 Y. Li, F. Xiong, Z. Wang, J. Yan, S. Wang, Z. Zhang and X. Jing, *Catal. Lett.*, 2022, **8**, 1–12.
39 A. Omidvar, B. Jaleh and M. Nasrollahzadeh, *J. Colloid Interface Sci.*, 2017, **496**, 44–50.
40 Y. Liu, X. Liu, W. Dong, L. Zhang, Q. Kong and W. Wang, *Sci. Rep.*, 2017, **7**, 12437.
41 M. Mohammadikish, *Ceram. Int.*, 2014, **40**, 1351–1358.
42 R. A. Reza and M. Ahmaruzzaman, *RSC Adv.*, 2015, **5**, 10575–10586.
43 M. Ghobadifard, P. V. Radovanovic and S. Mohebbi, *Appl. Organomet. Chem.*, 2022, **36**, e6612.
44 S. Yavari, N. M. Mahmodi, P. Teymouri, B. Shahmoradi and A. Maleki, *J. Taiwan Inst. Chem. Eng.*, 2016, **59**, 320–329.
45 B. Aslibeiki, N. Eskandarzadeh, H. Jalili, A. G. Varzaneh, P. Kameli, I. Orue, V. Chernenko, A. Hajalilou, L. Ferreira and M. Cruz, *Ceram. Int.*, 2022, **48**, 27995–28005.
46 A. H. Labulo, B. Omondi and V. O. Nyamori, *J. Mater. Sci.*, 2018, **53**, 15817–15836.
47 J. Moavi, F. Buazar and M. H. Sayahi, *Sci. Rep.*, 2021, **11**, 1–14.
48 S. Saire-Saire, E. C. Barbosa, D. Garcia, L. H. Andrade, S. Garcia-Segura, P. H. Camargo and H. Alarcon, *RSC Adv.*, 2019, **9**, 22116–22123.
49 Y. Omidi-Khaniabadi, A. Jafari, H. Nourmoradi, F. Taheri and S. Saeedi, *J. Adv. Environ. Health Res.*, 2015, **3**, 120–129.
50 R. J. Watts and A. L. Teel, *Water Res.*, 2019, **159**, 46–54.
51 H. Zhao, Y. Chen, Q. Peng, Q. Wang and G. Zhao, *Appl. Catal., B*, 2017, **203**, 127–137.
52 L. Xie, X. Liu, J. Chang, C. Zhang, Y. Li, H. Zhang, S. Zhan and W. Hu, *Chem. Eng. J.*, 2022, **428**, 131352.
53 Q. Peng, H. Zhao, L. Qian, Y. Wang and G. Zhao, *Appl. Catal., B*, 2015, **174**, 157–166.
54 F. E. Duran, D. M. de Araujo, C. do Nascimento Brito, E. V. Santos, S. O. Ganiyu and C. A. Martinez-Huitle, *J. Electroanal. Chem.*, 2018, **818**, 216–222.
55 A. Gopinath, L. Pisharody, A. Popat and P. Nidheesh, *Curr. Opin. Solid State Mater. Sci.*, 2022, **26**, 100981.
56 Y. H. Seo, M. Sung, Y.-K. Oh and J.-I. Han, *Bioresour. Technol.*, 2016, **200**, 1073–1075.
57 Y. Zhang, X. Kang, F. Zhen, Z. Wang, X. Kong and Y. Sun, *Biochem. Eng. J.*, 2022, **177**, 108198.
58 M. M. Phukan, R. S. Chutia, B. Konwar and R. Kataki, *Appl. Energy*, 2011, **88**, 3307–3312.
59 S. Huo, Z. Wang, F. Cui, B. Zou, P. Zhao and Z. Yuan, *Energies*, 2015, **8**, 8165–8174.
60 S. Das, S. Das and M. Ghangrekar, *Bioresour. Technol.*, 2021, **344**, 126218.
61 S. Kaur, M. Sarkar, R. B. Srivastava, H. K. Gogoi and M. C. Kalita, *New Biotechnol.*, 2012, **29**, 332–344.
62 Y.-H. Chen, B.-Y. Huang, T.-H. Chiang and T.-C. Tang, *Fuel*, 2012, **94**, 270–273.
63 J. M. Sonawane, A. K. Rai, M. Sharma, M. Tripathi and R. Prasad, *Sci. Total Environ.*, 2022, **824**, 153843.
64 Z. Yang, Y. Huang, X. Li, Z. Jiang, Y. Chen, S. Yang, H. F. Garces, Y. Sun and K. Yan, *Sep. Purif. Technol.*, 2022, **298**, 121535.
65 Y. Wang, Y. Liu, Z. Zhao, Z. Zheng, A. M. Balu, R. Luque and K. Yan, *Mater. Today*, 2023, **66**, 84–91.
66 B. Liu, M. Zhang, Y. Liu, Y. Wang and K. Yan, *Green Energy Environ.*, 2023, **8**, 874–882.

